IOP Conf. Series: Materials Science and Engineering **310** (2018) 012161 doi:10.1088/1757-899X/310/1/012161

Microstructure and Mechanical Behavior of Magnesium Alloy AZ91 Hybrid Composites

Sadanand Sarapure [1], B M Satish [2], B M Girish [3] and Basawaraj [4]

[1] Department of Mechanical Engineering, School of Engineering, Presidency University, Bangalore 560089, Karnataka, India
[2] Department of Mechanical Engineering, East Point College of Engineering and Technology, Bangalore, 560049, Karnataka, India
[3] Department of Mechanical Engineering,, Alliance College of Engineering and Design, Alliance University, Bangalore 562106, Karnataka, India
[4] Department of Aerospace Propulsion Technology, Center for Post-graduation Studies, Bangalore Region, Visvesvaraya Technological University, Muddenahalli – 562101, Karnataka, India

Corresponding author: Sadanand Sarapure, e-mail:sadanands2005@gmail.com

Abstract: AZ91 magnesium alloy hybrid composites reinforced with various ratios of SiC and graphite particles were synthesized by stir casting. The composites were prepared by varying the weight percentage of SiC and graphite particles each from 0 to 3 in steps of 1 weight percent. The average particle size of both the reinforcement particles was 27µm. The effect of reinforcement is discussed for both heat treated and non-heat treated composites and compared with unreinforced base alloy. The microstructure reveals that there is a nearly uniform dispersion of particles is the matrix. The density, hardness and ultimate tensile strength of the composite specimen increased as the percentage of reinforcement was increased both in heat treated and non-heat treated conditions. The percentage of elongation decreases as the reinforcement in the composites increased. SEM micrographs of the tensile fracture surfaces showed broken reinforcement particles on the fracture surface and evidence of 'pull outs', where graphite/SiC particles were previously embedded in the matrix.

1. Introduction

Metal Matrix Composites (MMCs) are materials that are gaining attraction for a large range of engineering applications as they combine high specific strength with good corrosion resistance. Given the factors of reinforcement quantity, form, and type, which can be varied, in addition to matrix characteristics, the composites have a enormous potential for being tailored for particular applications. Relatively higher cost is the factor that has restricted the widespread use of MMCs. The technical difficulties associated with attaining good wettability, uniform distribution of reinforcements and a low porosity material [1]. These materials can be candidates in aircraft, automotive, space and defense applications [2, 3] which demand lightweight, energy saving, inexpensive, high strength and high damping materials.

Magnesium matrix composites in the recent past are fast emerging as promising materials for light weight applications and are gaining increased importance in several applications [4-6]. Magnesium matrix composites reinforced by graphite particles are a unique class of advanced structure–function materials, and in order to offset the mechanical properties, SiC particles are also introduced into the composites. It is well known that the mechanical properties of magnesium alloys can be highly improved by adding SiC particles as an additional reinforcement [7-9]. Conversely, very limited information that is available on the aging behavior of discontinuously reinforced magnesium matrix composites, even though there is an increased attention due to their low density, higher specific properties and damping capacity [10-14]. Investigators [15, 16] have reported that the precipitation characteristics in the SiCp/Mg/6Zn composites were comparable to those found in SiC/Al composites, where noteworthy hardening has been achieved by artificial aging of SiCp/Mg/6Zn.
AZ91 magnesium alloy is the most popular and widely used among the magnesium casting alloy due to its combination of mechanical strength, ductility and castability. Moreover, AZ91 alloy is an age hardenable alloy, where cellular discontinuous precipitation at the grain boundary occurs simultaneously and competitively with the continuous precipitation within the grain over a wide temperature range. Although the utmost hardness attainable in AZ91 alloy is considerably lower than that in the precipitation-hardened aluminum alloys, the hardening response in the alloy is such as to have practical importance [17-19].

The aim of this study is to investigate the effect of SiC and graphite particles on microstructure and mechanical properties of SiC/graphite reinforced AZ91 alloy based hybrid composites for both as cast and age hardened conditions for different weight percentage of reinforcement in the composites. The mechanical behavior has been examined in terms of hardness and ultimate tensile strength, combined with microstructure observation using optical microscopy and failure analysis by scanning electron microscopy (SEM).

2. Experimental procedure

2.1 Composite fabrication.

The AZ91 magnesium alloy was chosen as the base matrix alloy in this study which has a chemical composition as given in Table 1.The vortex method of liquid metallurgy technique was used to prepare the composite specimens. Additional details about the materials preparation methodology is reported elsewhere by the same authors [20]. Hybrid reinforcements (SiC and graphite particles) varied from 1 to 3% in steps of 1 wt. %. The as-cast composites were solutionized at 415^{o}C for 4 hours followed by artificially aging at 168^{o}C for 16 hours.

2.2 Charecterisation.

The composite specimens were cut into required size for various tests. The examination of the microstructures was carried out and the samples were prepared as per ASTM E3 standard and chemical etching was done with Nital agent and the microstructure was studied under microscope (NIKON-Japan, ECLIPS 150 model). Energy dispersive X-ray spectroscope (EDS) was used to study micro-chemical characterization.

The densities of the composites were found by means of the Archimedes principle, using a Mettler Toledo AT261 Delta Range microbalance capable of measuring weight with an accuracy of 0.0001 g. As many as three specimens were tested for eachcase and the average values are presented in figure 5. A HBE−3000A Brinell hardness tester was adopted to measure the hardness of the composites. The applied load was 1000 kN, and the holding time was 15 s. The diameter of the steel sphere used was 10 mm. Three spots on a sample were tested, and the reported results are the average of readings obtained. The tensile tests were conducted in accordance with ASTM E8 – 82 standards. As many as three specimens were tested for each case and the average values are presented. The test specimens were subjected to homogeneous and uniaxial tensile stresses in an universal testing machine.

Scanning electron microscope (SEM) was used for the study of tensile fracture surface to: (a) determine the macroscopic fracture mode, and (b) characterize the fine scale topography and microscopic mechanisms governing fracture. The primary distinction between the macroscopic mode and microscopic mode and resultant mechanisms governing fracture is based on the magnification level at which the observations are made.

3. Results and discussion

3.1 Microstructure analysis of the as cast and aged composite specimens.
The chemical composition of base AZ91 alloy is shown in Table 1.

Table 1. Chemical composition of AZ91 alloy(wt %)

Al	Zn	Mn	Si	Cu	Fe	Ni	Mg
9.0	1.0	0.035	0.035	0.005	0.005	0.001	Remaining

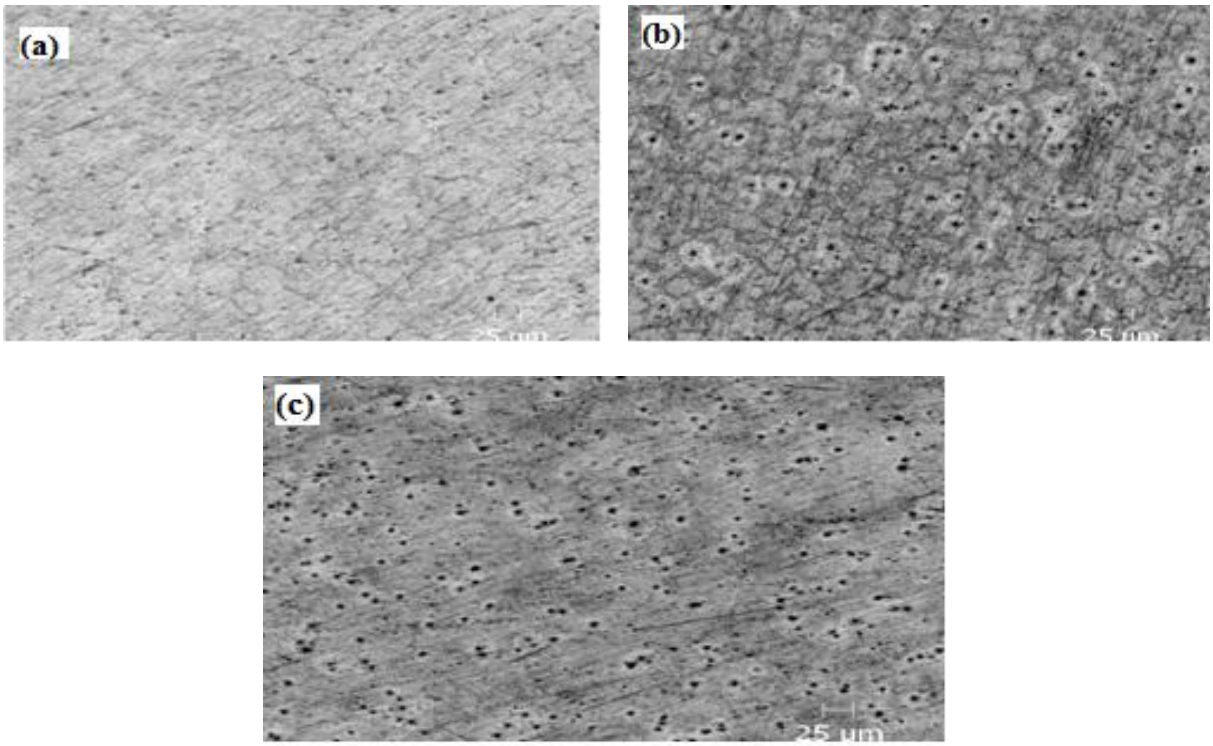

Figure 1. Optical micrographs of un-etched as cast composites (a) 1wt.% of reinforcement, (b) 2wt. % of reinforcement, and (c) 3wt. % of reinforcement (100X).

Figure 1a, 1b, and 1c shows the microstructure of the hybrid composite reinforced with 1% SiC and1% graphite, 2% SiC and 2% graphite, and 3% SiC and 3% graphite particles respectively. The optical microscopy studies show a uniform distribution of reinforcement in the matrix. Silicon carbide and graphite particle reinforcements remain well bonded to the matrix and no defects were found . It follows from the microstructures provided in figure 2a, and 2b that the grains are very clear for the base alloy and the reinforcement particles are uniformly located both at the grain

boundaries and inside the primary α-Mg grains in the composite. It is found that the addition of the reinforcement particles significantly decreases the grain size of the matrix in the composite. The refinement of grains in the matrix is attributed to the heterogeneous nucleation of the primary Mg phase. Certain crystallographic orientation relationships between the particle and the matrix, and the restricted growth of Mg grains by SiC_p during solidification further contribute to the reduction in grain size[21]. The alloy consists of α-matrix grains (solid solution of Al and Zn in Mg) and $Mg_{17}Al_{12}$ (β-phase) intermetallic precipitate. From figure 3, it can be noticed that there is massive amount of precipitates of $Mg_{17}Al_{12}$ (β-phase) in aged composite specimens.

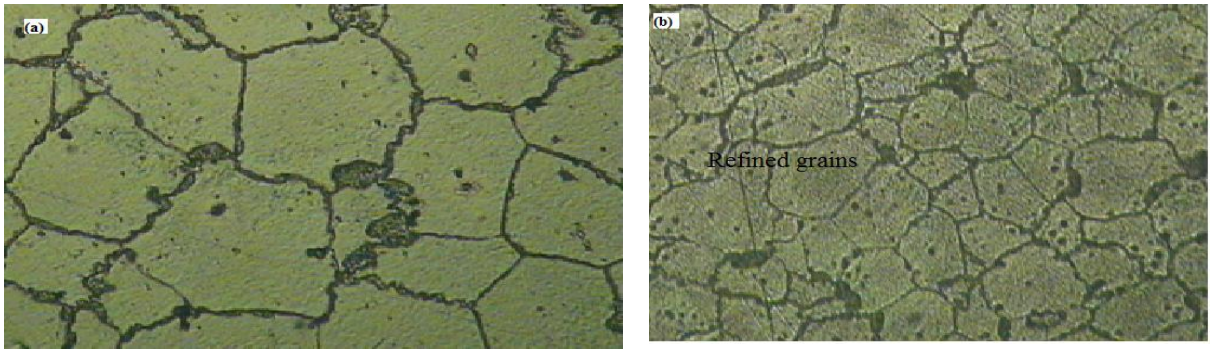

Figure 2. Optical micrographs of etched (a) as cast unreinforced alloy and (b) as cast 3 wt. % Composites.

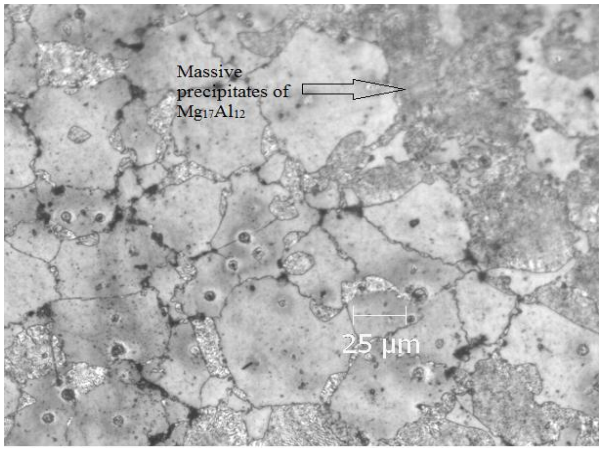

Figure 3. Optical micrograph for solutionized and aged composite with 1 wt. % reinforcement (200X).

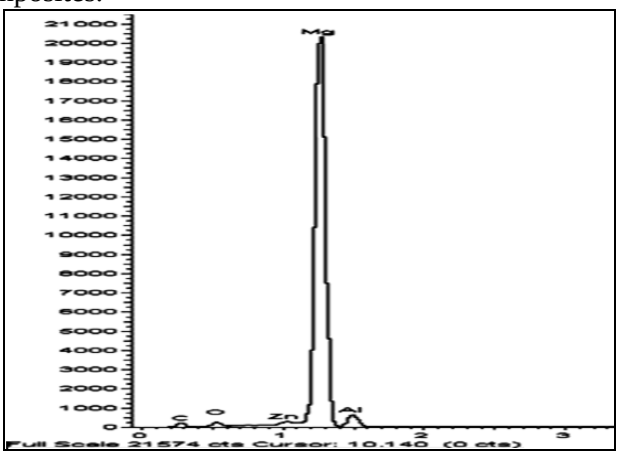

Figure 4. EDS spectrum of AZ alloy composite with 3 wt. % reinforcement.

Figure 4 shows EDS spectrum of 3 weight percent composite material and the corresponding chemical analysis is given in Table 2.

Table 2. Micro-chemical analysis from EDS spectrum of the 3% SiC and 3% graphite reinforced composite.

C	O	Mg	Al	Si	Zn
6.05	3.42	80.33	7.6	2.1	0.5

3.2 Density.

The density values were measured using both Archimedes' principle (ρ_{mc}) and the rule of mixtures (ρ_{th}) for the base alloy and the composites. The density values of the composites (figure 5) are found to increase with the increasing mass fraction of SiCp, which is due to the presence of higher density SiCp, when compared with AZ91[22]. The density measurements involved weighing of samples in air and when immersed in distilled water. The theoretical density (ρ_{th}) was obtained using rule of mixture as mentioned below:

$$\rho_{th} = \rho_m V_m + \rho_{r1} V_{r1} + \rho_{r2} V_{r2}$$

Where $V_m = 1 - (V_{r1} + V_{r2})$ is the volume fraction of the matrix.

Density measurement values were compared with the theoretical density values. The percentage of deviation in the values of experimental density was found to be less than 1%.

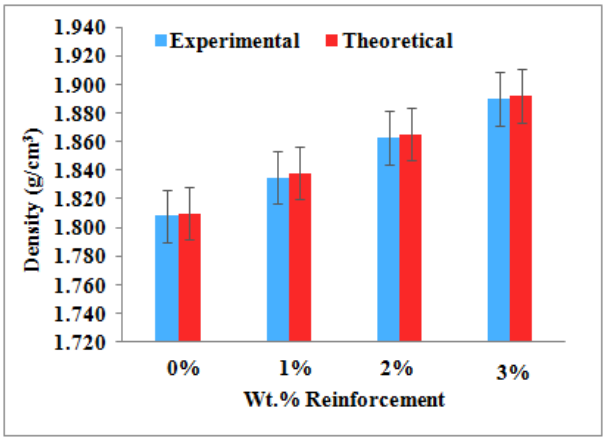

Figure 5. Figure showing the variation of density v/s wt. % reinforcement.

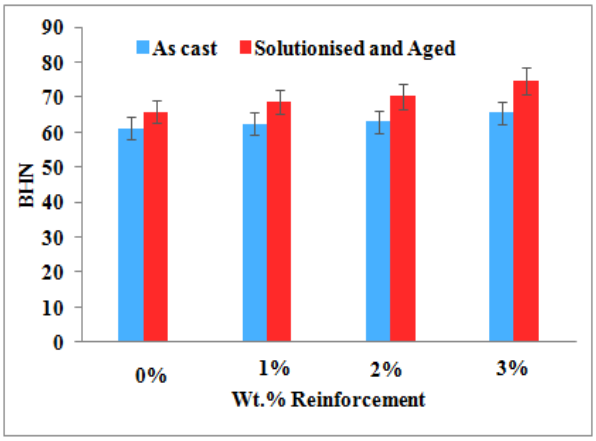

Figure 6. Figure showing the variation of Brinell hardness number v/s wt. % reinforcement.

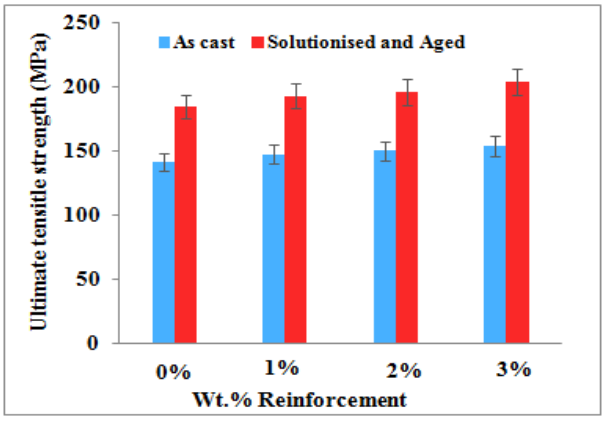

Figure 7. Figure showing the variation of Ultimate Tensile Strength (UTS) v/s wt. % reinforcement.

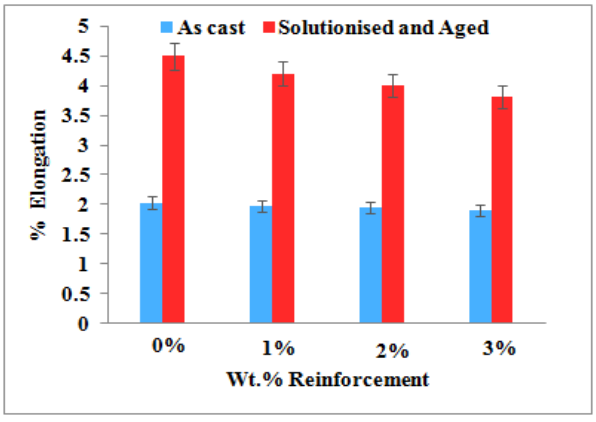

Figure 8. Figure showing the variation of percentage of elongations v/s wt. % reinforcement.

3.3 Mechanical properties.

3.3.1 Hardness. The figure 6 shows the variation of hardness verses weight percent of reinforcement. It is observed that there is an increase in the hardness due to the hard and uniform distribution of SiC_p. There is an increase in hardness when the content of reinforcement is increased from 0 to 3 weight percent. It is also observed that the hardness of aged composites is more compared with as cast composites. This is due to the precipitation of hard secondary phase $Mg_{17}Al_{12}$ (β-phase). The higher hardness is found in case of aged composite, because of increased grain boundary area in fine grained materials; hence, the ejection of aluminium from supersaturated solution is fast and the same reactions with matrix elements form an equilibrium compound spread over the matrix. During aging, the β-phase precipitates form as discontinuous precipitation. The discontinuous precipitation is the cellular growth of alternating layers of β-phase where the continuous precipitation region ceases its growth early in the precipitation process. At higher magnification, the fine precipitates widely spread throughout the grain is clearly visible in figure 3. These fine precipitates throughout the matrix are responsible for the increase in the hardness of the aged composite samples. Similar observations were made by Thirumurugan et.al. [23].

3.3.2 Tensile Strength. The figure 7 shows the variation of ultimate tensile strength (UTS) with respect to the variation in weight percent reinforcement for both as cast and aged samples. It is observed that the UTS is increased as the weight percent of reinforcement is increased. This is a clear indication of strength to the matrix by the uniform distribution of SiC and graphite particulate reinforcement in the composites. There is a 9% of increase in UTS as the weight percent of reinforcement is increased from 0 to 3. It is also observed that for aged sample with 3 weight percent reinforcement , there is significant increase in the UTS of about 45% when compared to unreinforced as cast sample which is mainly due to the precipitation of hard secondary phase in the matrix for aged composite and also the effect of grain refinement due to reinforcement particles.

The effect of SiC and graphite particle content on the ductility of both as cast and aged AZ91alloy based particulate reinforced hybrid composites (measured in terms of percentage elongation) are shown in figure 8. It can be seen that the ductility of the composites decreases significantly with the increase in reinforcement content. The ductility drops by about 6% as the percentage of reinforcement content is increased from 0 to 3. This decrease in ductility in comparison with the matrix alloy is a most commonly encountered disadvantage in dis-continuously reinforced MMCs. Graphite particles can effectively hinder grain growth , the higher the graphite articles content, the weaker the grain growth and hence presence of graphite particles will promote finer grains sizes. The variation of tensile properties is related to grain size and graphite particle volume fraction, small grain size leads to high strength. It was verified from the work carried out by Arsenault RJ et al,[24] that the micro plasticity takes place in the metal matrix composites due to stress concentrations in the matrix at the poles of the reinforcement and/or at sharp corners of the reinforcing particles. Hence, the introduction of this hard secondary ceramic phase creates slip regions. Moreover, the reinforcing particulates resist the passage of dislocations either by creating stress fields in the matrix or by inducing large differences in the elastic behavior between the matrix and the dispersoid.

Figure 9 shows the engineering stress - strain curve for both as cast and aged composites containing reinforcement in different percentages. It is evident from the stress-strain curve for both the as cast and aged composites that the ultimate tensile strength is increasing with increase in reinforcement content but the maximum strain is decreased with increase in the reinforcement content. The strength of the artificial aging AZ91D/SiCp/graphite composite is better than as cast composite and unreinforced monolithic magnesium alloy (AZ91D). The strengthening effect of matrix (magnesium alloy) is due to dislocation and precipitation hardening. The strength of magnesium is highly sensitive to its grain size. Grain refinement due to heat treatment contributes to

the great strength at room temperature for magnesium alloy composite. The finer grain size in the composite specimens results in increase in the area of grain boundary. Thus increasing the strength as the amount of material allowed to diffuse rapidly along the grain boundaries would be increasing[25].

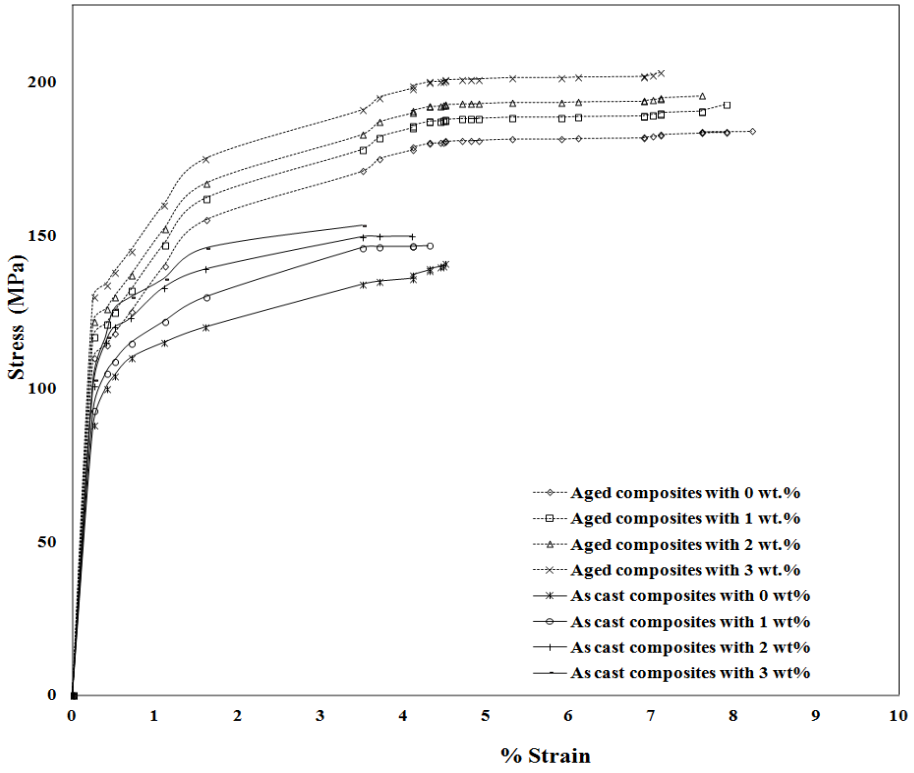

Figure 9. Figure showing the engineering Stress - Strain curve for both as cast and aged composites with various reinforcement contents.

3.4 Failure analysis and Fractography.

Figure 10 shows the SEM image of the fractured surface of as cast composite with 3 wt. % reinforcement. Brittle appearance was noticed on the fracture surface of the test specimen at macroscopic scale (figure 10a) and also an inter-granular fracture was observed when viewed at higher magnification (figure 10d).Also it can be seen in the SEM images of the fractured surface (figure 10b) that the existence of group of fine microscopic cracks spread randomly. The crack path morphology of macroscopic crack was essentially non-linear as it propagated through the alloy matrix and it is revealed at the higher magnifications (figure 10c). It was also observed that there is a random distribution of very fine microscopic cracks surrounding the macroscopic crack. SEM images of fracture surface at higher magnifications revealed a group of dimples of varying shape and size immediately adjoining to the fine microscopic cracks as well as macroscopic cracks, indicating mixed brittle and ductile failure mechanisms.

It is clear from figure 10d that the fractography of as cast composites possesses the smallest deformation zone, exhibiting an entire inter-granular fracture feature, and also the lowest tensile strength and elongation when compared to aged counterparts. The lack of development of ductile dimples, as the principal fracture mode, is essentially because of presence of discontinuous SiC reinforcements in the composite matrix causing limited plastic flow and not limited to ductility of the matrix of magnesium alloy.

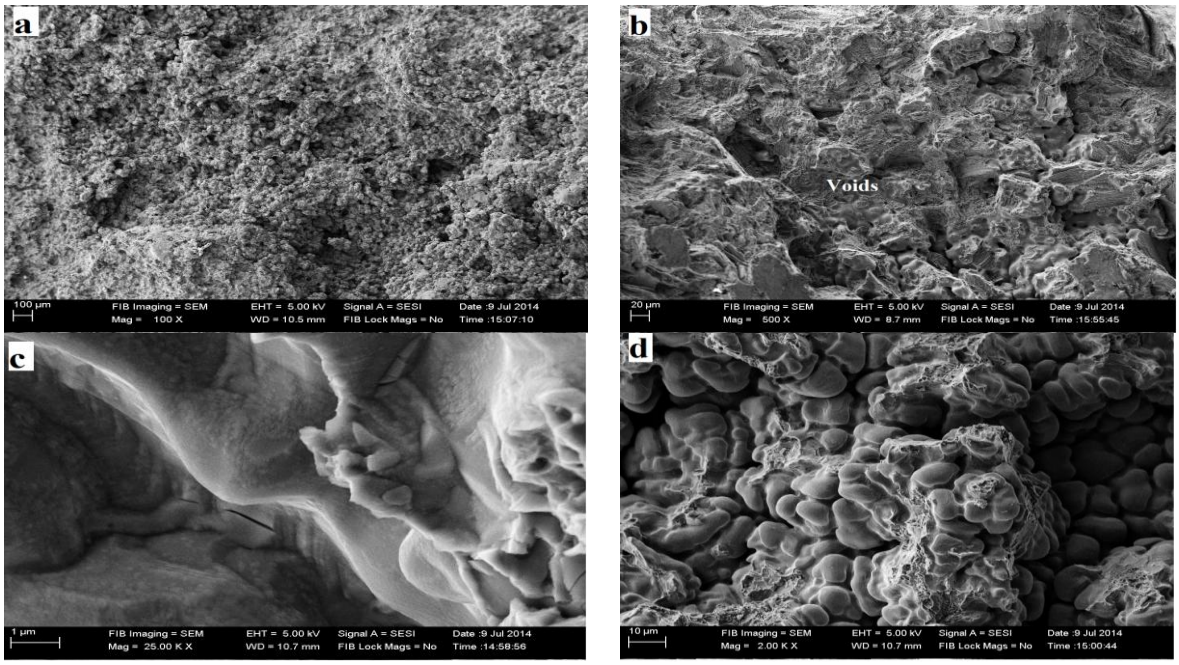

Figure 10.SEM images of the tensile fracture surface of the as cast AZ91 alloy with 3 wt. % reinforcement (a) overload region, (b) Varying sized Voids intermingled with dimples, (c) Cracked reinforcing silicon carbide and (d) Smallest deformation with almost intergranular fracture feature.

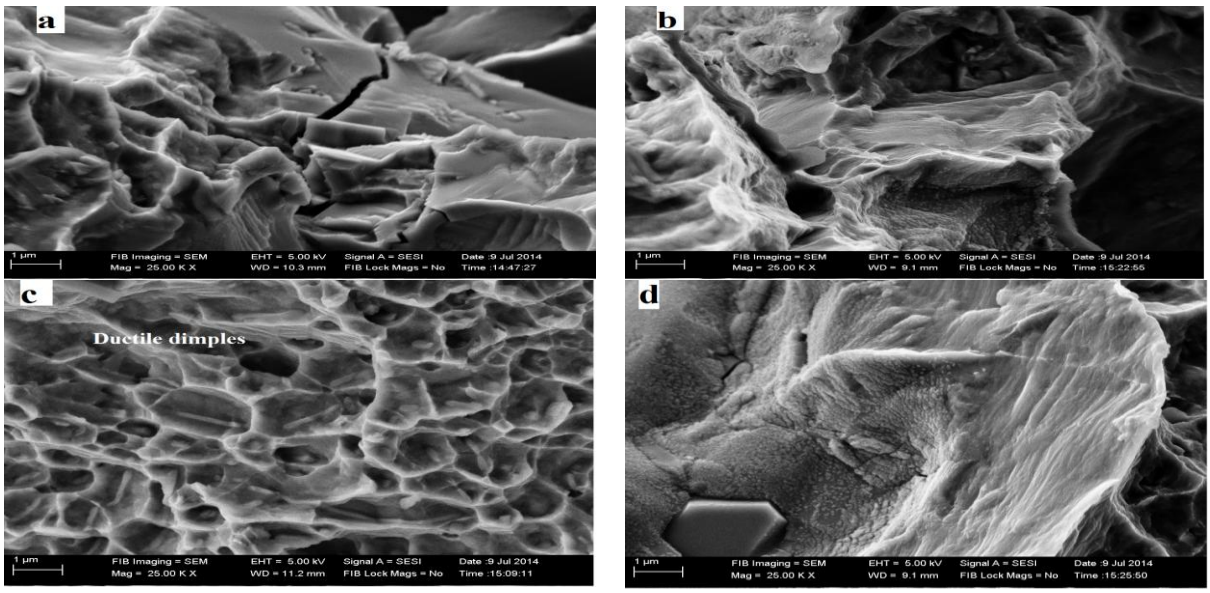

Figure 11.SEM of the tensile fracture surfaces of the Aged AZ91 alloy composites with 3 wt. % reinforcement showing (a) mixed mode failure - failure of reinforcement is brittle and failure of matrix is ductile (b) deboning at the particulate–matrix interface, (c) presence of ductile dimples surrounding the reinforcing SiC particulates, (d) particulate agglomeration of on fracture surface.

During the process of tensile deformation a gradual increase in strain causes fracture of the larger sized SiC particles first, and then the fracture of the smaller sized SiC particles occurs. As the flaw/deffect size in a particle is directly proportional to its size and hence the tendency for the larger particles to fracture at a lesser stress than the smaller particles.

In such regions where there are SiC particulate agglomeration/clusters, the short inter-particle distance provides linkage between the adjacent voids and microscopic cracks as a direct result of reduced propagation distances amid the cracked SiC particles. The fracture surfaces observations reveal that the plane of fracture for the cracked SiC particles is basically normal to the axis of loading, signifying the importance of normal stress in causing particle fracture. The overall lower ductility of the composite compared to the unreinforced alloy contributed to the failure of the reinforcing SiC particles both by cracking as well as de-bonding at metal matrix interfaces.

However there were more indications of comparatively ductile mode of fracture in case of aged samples as shown in figure 11 a-d. Observations on a macroscopic scale indicated that, the fracture was basically perpendicular to the far-field stress axis (figure 11a). And relatively rough fracture surface was noticed at the microscopic scale (figure 11b).

When the fracture surfaces were observed under high magnifications, the fracture surface revealed both fractured silicon carbide particles (figure 11d) surrounded by tear ridges indicating pockets of ductile regions.

The ductile failure can be safely related to ridges and also the pockets of dimples of varying size and shape in the tensile fracture surface indicate ductile failure. The region of overload on the tensile fracture surface can be seen in figure 11a. A population of fine microscopic voids can be noticed on the fracture surface of matrix of as cast composite (figure 11b). These voids were intermingled with clearly distinct regions containing dimples (figure 11c). At the higher acceptable magnifications of the SEM images of this region noticeably reveals voids of varying size intermingled with dimples of varying shape and size, indication of failure mechanisms is locally ductile.

However the clear cracked reinforcing particles observed at higher magnifications in this specific region were (figure 11d) indication of failure mechanisms as locally brittle. The presence of fundamentally elastically deforming, brittle and hard reinforcing SiC particulates imposes restriction on the mechanical deformation of the plastically deforming, ductile and soft metal matrix of magnesium alloy and this results in the development of a triaxial stress state in the matrix of magnesium alloy. This causes reduction in the flow stress of the composites[26, 27].

4. Conclusions

Magnesium alloy AZ91 matrix ohybrid composites reinforced withosilicon carbide (SiC) and graphite (Gr) oparticles were successfully oprepared using stir casting otechnique with various volumeo percentages. Hardness and tensile oproperties of as cast and aged ocomposites were oinvestigated. From the present oinvestigation the following conclusions may be odrawn:

1. The sizes of the grains in the composite alloy were smaller. The reinforcements were found to be distributed uniformly in the alloy microstructure. In case of aged composites, precipitation of hard intermetalic compound β-phase ($Mg_{17}Al_{12}$) were observed
2. The hardness of the composite alloy was high when compared with unreinforced monolithic counter parts both in as cast and aged conditions. The hardness found to be increase with increase in reinforcement content.
3. Similar observation is found with the ultimate tensile strength (UTS). It was found that UTS increase with increase in reinforcement content both in as cast and aged composites.
4. Because of the hindering effect of micron particle mainly SiCp on dislocations, the dislocation density around particles increase during room temperature tensile process, which contribute to the enhancement of tensile strength.
5. Morphology of tensile fracture surface revealed an overall brittle in appearance macroscopically and features brittle and ductile failure mechanisms noticed microscopically.

References:

[1] J Hashmi, L Looney, M S J Hashmi, 1999, *J. of Mater. Proc. Tech*. **92-93**, 1-7.
[2] S Suresha, B K Sridhara, 2010, *Mater. Des*. **31**, 1804–1812.
[3] J H Gu, X N Zhang, M Y Gu, 2004, *J. Alloys Compd.* **385**, 104–108.
[4] H J Li, Z J Li, L H Qi, H Oy, 2009, *Scripta Mater.* **61**, 512–515.
[5] X J Wang, K Wu, H F Zhang, W X Huang, H Chang, W M Gan, M Y Zheng, D L Peng, 2007, *Mater. Sci. Eng. A* **465**, 78–84.
[6] H Ferkel, B L Mordike, 2001, *Mater. Sci. Eng. A,* **298**, 193–199.
[7] P Poddar, V C Srivastava, P K De, K L Sahoo, 2007, *Mater. Sci. Eng. A,* **460–461**,357–364.
[8] G Cao, H Konishi, X Li, 2008, *Mater. Sci. Eng. A* **486**, 357–362.
[9] K Wu, K K Deng, K B Nie, Y W Wu, X J Wang, X S Hu, M Y Zheng, 2010, *Mater. Des.* **31**, 3929–3932.
[10] K U Kainer, 1991, *Mater. Sci. Eng. A,* **135**, 243-246.
[11] V Laurent, P Jarry, G Regazzoni, D Apelian, 1992, *J. Mater. Sci.* **27**, 4447-4459.
[12] T Wada, T Shinkawa, S Kamado, Y Kojima, 1995, *J. Jpn. Inst. Light Metals*, **45**, 504-509.
[13] A Luo, 1995, *Metall. Mater. Trans. A*, **26A**, 2445-2455.
[14] M Zheng, K Wu, C K Yao, 2001, *Mater. Sci. Eng. A*, **318**, 50-56.
[15] P K Chaudhury, H J Rack, 1991, *J.Mater. Sci.* **26**, 2893-2899.
[16] P K Chaudhury, H J Rack, B A Mikucki, 1991, *J. Mater. Sci*. **26**, 2343-2347.
[17] A F Crawley, 1974, *Acta Metall.*, **22**, 557-562.
[18] A F Crawley, B Lagowski, 1974, *Metall. Trans.* **5**, 949-951.
[19] S Celotto, 2000, *Acta Mater.* **48**, 1775-1787.
[20] B M Girish, B M Satish, Sadanand Sarapure, D R Somashekar and Basawaraj, 2015, *Tribol. Trans*., **58**, 481–89.
[21] P Poddar, V C Srivastava, P K De, K L Sahoo, 2007, *Mater. Sci.Eng. A*, **460-461**,357-364.
[22] G Gertsberg, E Aghion, A Kaya, D Eliezer, 2009, *J. Mater. Eng.Perform.***18**, 886-892.
[23] M Thirumurugan, S Kumaran, 2013, *Trans. Nonferrous Met. Soc. China*, **23**, 1595−1601.
[24] R J Arsenault, L Wang and C R Feng, 1991, *Acta Metallurgica*, **39**, 47-57.
[25] T Mochida, M Taya, D J Lloyd, 1991, *Materials Transactions, Japan Institute of Metals,* **32 (10)**, 931–942.
[26] M Taya, T Mori, 1987, *Acta Metallurgica*, **35**,155–163.
[27] S Aravindan, P V Rao, K Ponappa, 2015, *Journal of Magnesium and Alloys*, **3**, 52-62.